Structure and Activity Analysis of Two Spider Toxins That Alter Sodium Channel Inactivation Kinetics

10 AUTHORS, INCLUDING:

Maria Elena De Lima
Federal University of Minas Gerais
84 PUBLICATIONS **1,335** CITATIONS

SEE PROFILE

Jader Cruz
Federal University of Minas Gerais
110 PUBLICATIONS **1,749** CITATIONS

SEE PROFILE

Carlos Henrique Inacio Ramos
University of Campinas
107 PUBLICATIONS **1,722** CITATIONS

SEE PROFILE

Paulo Beirão
Federal University of Minas Gerais
45 PUBLICATIONS **821** CITATIONS

SEE PROFILE

Structure and Activity Analysis of Two Spider Toxins That Alter Sodium Channel Inactivation Kinetics[†]

Alessandra Matavel,[‡,§] Cécile Fleury,[‡,§,||] Leida C. Oliveira,[‡] Franck Molina,[||] Maria Elena de Lima,[‡] Jader S. Cruz,[‡] Marta N. Cordeiro,[⊥] Michael Richardson,[⊥] Carlos H. I. Ramos,[#] and Paulo S. L. Beirão*,[‡]

Department of Biochemistry and Immunology, Instituto de Ciências Biológicas, Universidade Federal de Minas Gerais, Avenida Antônio Carlos 6627, CEP 31270-901 Belo Horizonte, MG, Brazil, Centro de Pesquisa e Desenvolvimento Carlos Ribeiro Diniz, Fundação Ezequiel Dias, Belo Horizonte, Brazil, Sysdiag, CNRS FRE 3009, 1682 rue de la Valsière, CS 61003, 34184 Montpellier CEDEX 4, France, and Department of Organic Chemistry, Instituto de Química, Universidade Estadual de Campinas, Campinas, Brazil

Received November 21, 2008; Revised Manuscript Received February 17, 2009

ABSTRACT: In this work, *Phoneutria nigriventer* toxins PnTx2−5 and PnTx2−6 were shown to markedly delay the fast inactivation kinetics of neuronal-type sodium channels. Furthermore, our data show that they have significant differences in their interaction with the channel. PnTx2−6 has an affinity 6 times higher than that of PnTx2−5, and its effects are not reversible within 10−15 min of washing. PnTx2−6 partially (59%) competes with the scorpion α-toxin AaHII, but not with the scorpion β-toxin CssIV, thus suggesting a mode of action similar to that of site 3 toxins. However, PnTx2−6 is not removed by strong depolarizing pulses, as in the known site 3 toxins. We have also established the correct PnTx2−5 amino acid sequence and confirmed the sequence of PnTx2−6, in both cases establishing that the cysteines are in their oxidized form. A structural model of each toxin is proposed. They show structures with poor α-helix content. The model is supported by experimental and theoretical tests. A likely binding region on PnTx2−5 and PnTx2−6 is proposed on the basis of their different affinities and sequence differences.

Peptide toxins were selected over millions of years to act on vital processes to kill or paralyze prey or predators. This natural selection provided an assortment of molecules capable of acting at low concentrations on ion channels, either inhibiting their conduction pathway or altering their kinetics (*1*). The latter type of toxins is proving to be a useful tool for investigating the molecular mechanisms of ion channel gating and has provided valuable information about this poorly understood process (see ref *2* as an example). At least six toxin binding sites have been characterized in the mammalian sodium channel, most of them affecting its kinetics. Site 3 is known to be occupied by peptide toxins that originated from scorpion venom (scorpion α-toxins) and from sea anemone, whereas site 4 is occupied by scorpion β-toxins (*3*). More recently, some spider toxins have also been shown to alter the kinetics of sodium channels. In contrast with the scorpion and anemone toxins, little is known about their molecular mechanism and binding sites (*4*).

In this paper, we have studied two homologous toxins from the Brazilian spider *Phoneutria nigriventer*, whose effects can account for the major symptoms of envenomation caused by that spider, which comprise hyperexcitation, salivation, lachrymation, and priapism. At the cellular level, these toxins have been shown to have complex effects on sodium channel kinetics, inhibiting its inactivation and shifting the activation voltage dependence toward negative potentials (*4, 5*), effects that correspond to the action of scorpion α- and β-toxins, respectively. Those two toxins, named *P. nigriventer* toxins Tx2−5 (PnTx2−5)[1] and Tx2−6 (PnTx2−6), are similar in primary sequence, and their in vivo activities also resemble those produced by scorpion toxins, except for the conspicuous priapism. However, more detailed studies at the cellular level were still required to characterize their mechanisms of action. In this work, we present a detailed and ample set of results that indicates that these toxins act on neuronal sodium channels by binding to the overlapping site with scorpion α-toxins and by a similar mechanism.

MATERIALS AND METHODS

Electrophysiology. The GH3 (ATCC, Manassas, VA) cell line was used for the electrophysiology assays. The cells were kept in Dubelco's modified Eagle's medium (DMEM, Gibco)

[1] Abbreviations: AaHII, *Androctonus autralis* Hector toxin II; BSA, bovine serum albumin; CD, circular dichroism; Css IV, *Centruroides suffusus suffusus* toxin IV; EGTA, [ethylene bis(oxyethylenenitrilo)]tetraacetic acid; FPLC, fast protein liquid chromatography; HEPES, 4-(2-hydroxyethyl)-1-piperazineethanesulfonic acid); HPLC, high-performance liquid chromatography; ICK motif, inhibitory cystine knot motif; PnTx2−5, *P. nigriventer* toxin Tx2−5; PnTx2−6, *P. nigriventer* toxin Tx2−6; SEM, standard error of the mean; TEA, tetraethylammonium; UV, ultraviolet.
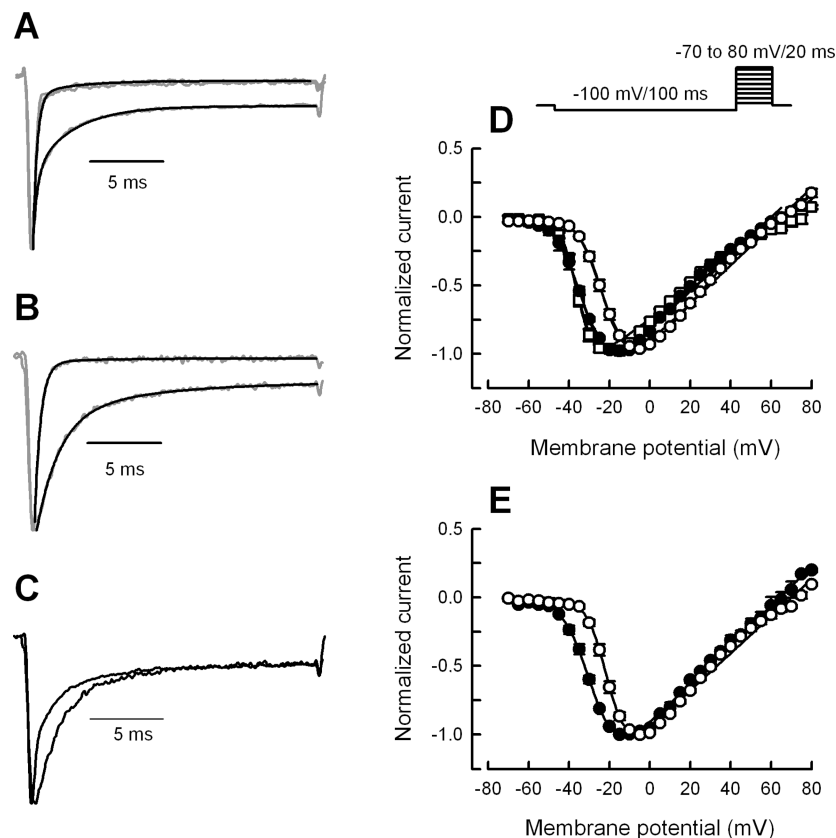
FIGURE 1: Effect of PnTx2−5 and PnTx2−6. (A) Superimposed records (gray lines) obtained from the same cell at 0 mV in the absence or presence of 400 nM PnTx2−5 and 5 min after washing. The latter record is almost identical with the control. The black line shows the curve obtained by fitting the inactivation kinetics, as described in Materials and Methods. (B) Same as panel A, with and without 100 nM PnTx2−6. (C) The records in the presence of PnTx2−5 and PnTx2−6 are superimposed to stress the difference in their effects. (D) Normalized I−V curves in the absence (○) or presence of 400 nM PnTx2−5 (●) and 5 min after washout (□). (E) Normalized I−V curves in the absence (○) and presence of 100 nM PnTx2−6 (●). The pulse protocol of the I−V curves is shown above panel D. The I−V curve was fitted with the equation $I_{Na} = g_{Na(Max)} \times (V_M - V_R)/\{1 + \exp[(V_g - V_M)/K_g]\}$, where I_{Na} is the current at each point, $g_{Na(Max)}$ is the fitted maximal conductance, V_M is the membrane potential, V_R is the reversal potential, V_g is the voltage which activates half of the maximal conductance, and K_g is the slope factor.

supplemented with 10% fetal bovine serum (Cultilab), 10 units/mL penicillin, and 10 μg/mL streptomycin. The cells were plated 2−5 days before the experiment, and 24−48 h before the experiment, the concentrations of KCl and CaCl$_2$ in the culture medium were increased to 10 and 9.3 mM, respectively, to increase the level of sodium channel expression (6). Macroscopic Na$^+$ currents were recorded at room temperature (22−25 °C) in the whole-cell patch clamp configuration (7) using an EPC-9 amplifier (Heka Instruments). Currents were low-pass filtered (Bessel) at a cutoff frequency of 10 KHz, acquired at 20−25 KHz, and digitally stored in a Power-Mac computer. The P/4 protocol was used for linear leak and capacitance subtraction. Patch pipettes were made with soft glass capillaries using a vertical pipet puller (Narishige) and had resistances between 2 and 4 MΩ. The pipettes were filled with internal solution 1 [10 mM NaCl, 20 mM TEA-Cl, 10 mM EGTA, 90 mM CsF, 20 mM CsOH, and 10 mM HEPES (pH 7.2) with CsOH] for experiments on PnTx2−5 or internal solution 2 [10 mM NaCl, 35 mM TEA-Cl, 5 mM EGTA, 100 mM CsF, and 10 mM HEPES (pH 7.2) with CsOH] for experiments with PnTx2−6. TEA-Cl and cesium were used to suppress K$^+$ currents. The external solution contained 140 mM NaCl, 5 mM CsCl, 2 mM MgCl$_2$, 0.1 mM CdCl$_2$, 1 mM CaCl$_2$, 5 mM glucose, and 10 mM HEPES (pH 7.4) with NaOH. Cadmium was used to block Ca^{2+} channels. Throughout the

experiment, the cell under investigation was externally perfused via a 0.1 mm diameter pipet that was placed visually next to it. The perfusion was performed with the external solution containing 0.1% bovine serum albumin (BSA), to avoid adsorption of the toxin. BSA had no effect on the Na$^+$ current. When appropriate, the perfusing solution was switched to an equal solution containing the toxin at the desired concentration. The effectiveness of the perfusion was checked beforehand by using a Na-free external solution. Under that condition, the inward current completely disappeared within 2 s. All reagents were of analytical grade.

Data Analysis. For the kinetic analysis of Na$^+$ current inactivation, the decay of the current at a membrane potential of 0 mV was fitted with an exponential function with one or two time constants:

$$f(x) = a \exp(-T/\tau_f) + c \qquad (1)$$

$$f(x) = a \exp(-T/\tau_f) + b \exp(-T/\tau_s) + c \qquad (2)$$

where T is the time from the peak of the current and a and b are the proportions of the current that decays with time constants τ_f and τ_s, respectively.

Toxin Purification and Quantification. The PnTx2 fraction was purified by gel filtration chromatography in gel and reversed-phase chromatography in FPLC (8) from a soluble
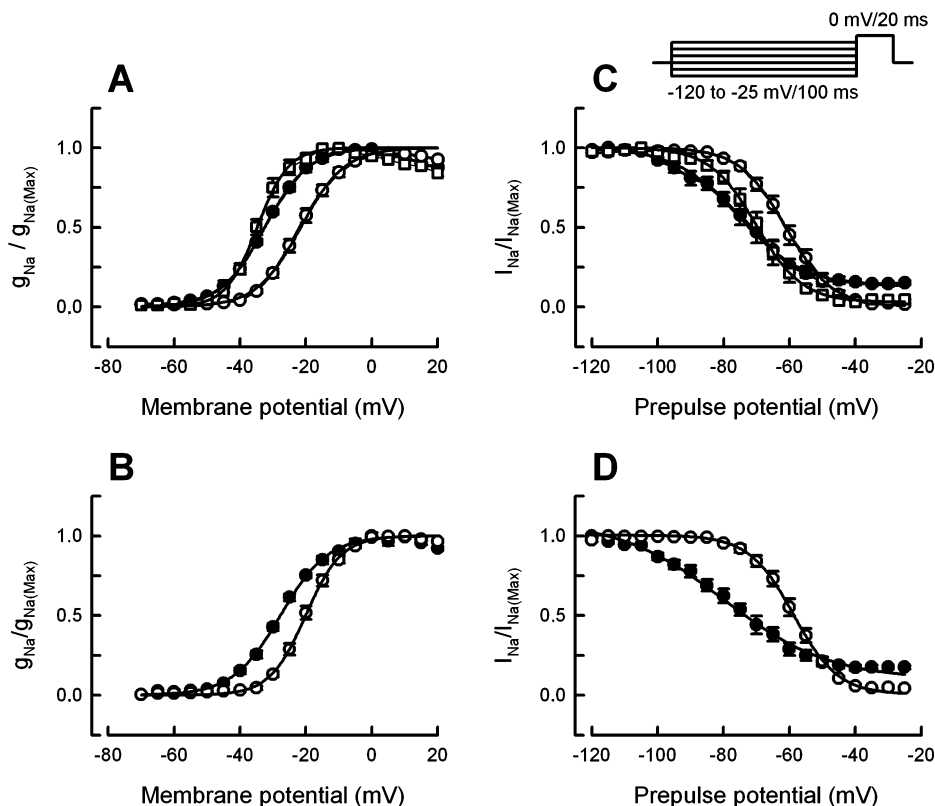
FIGURE 2: Effect on the voltage dependence of the peak conductance of 100 nM PnTx2−6 (A) and 400 nM PnTx2−5 (B). The conductance at each point was calculated using the equation $g_{Na} = I_{Na}/(V_M − V_R)$ and fitted with a Boltzmann equation: $g_{Na}/g_{Na(Max)} = \{1 + \exp[(V_g − V_M)/K_g]\}^{-1}$. The right panel shows the voltage dependence of steady-state inactivation with 100 nM PnTx2−6 (C) and 400 nM PnTx2−5 (D). The pulse protocol used to measure the voltage dependence of steady-state inactivation is shown. The steady-state inactivation data were fitted with the equation $h_\infty = a\{1 + \exp[(V − V_h)/K_h]\}^{-1} + b$, where V is the prepulse membrane potential, V_h is the voltage that inactivates half of the maximal current, and K_h is the inactivation slope factor. Parameters a and b reflect the proportion of inactivating and noninactivating channels, respectively: control (○), in the presence of the toxin (●), and 5 min after washout (□).

fraction of the total venom of the *P. nigriventer* spider. Isoforms PnTx2−5 and PnTx2−6 were separated by reversed-phase chromatography via HPLC (*9*). The purity of the toxins was verified by mass spectrometry (Q-Tof, Micromass, Manchester, U.K.). To quantify the toxin concentration, we calculated the molar extinction coefficient at 280 nm of each toxin in its denatured form, on the basis of the respective amino acid content. The ε was calculated with the equation $\varepsilon_{280} = (\text{number of W}) \times 5690 + (\text{number of Y}) \times 1280 + (\text{number of C−C}) \times 120$ (*10*). Since it has been shown in native proteins that calculated extinction coefficients were accurate within an average of 5% error (*11*), we used this value throughout this work.

Tryptophan Fluorescence and Circular Dichroism (CD). Fluorescence records of PnTx2−6 were obtained with an ABL2 Spectronic fluorometer (Applied Biosystems, Foster City, CA) in quartz cuvettes with a path length of 1 cm. The sample was excited at 280 nm and the emission spectrum collected at 300−450 nm at 20 °C. The CD spectrum of PnTx2−6 was obtained with a spectropolarimeter (Jasco J-810) in a quartz cuvette with a path length of 1 cm with UV light from 190 to 260 nm at 23 °C. The toxin was diluted in water. The data were obtained at 0.5 nm intervals at 50 nm/min. All CD spectra are averages of 20 scans. The baseline under each condition was subtracted from the spectrum with the toxin.

Binding Assay. To identify the PnTx2−6 binding site on sodium channels, we performed competition assays using typical scorpion toxins that bind to site 3 (AaHII from

Androctonus australis Hector) and site 4 (CssIV from *Centruroides suffusus suffusus*). These toxins (5 nmol) were radiolabeled by the lactoperoxidase method with 0.5 mCi of [125]I (Amersham Pharmacia Biotech) as described by Rochat and collaborators (*12*). To perform the experiments, we used either 5 µg of synaptosomes from rat brain (*13*) or 50 µg of total synaptosomal preparation (P2) (*14*). The protein concentration was determined by the method of Lowry (*15*). The tissue was incubated (30−40 min at 37 °C) in a medium containing 10^{-10} M radiolabeled toxin ([125I]Aa-HII or [125I]CssIV), alone or with a competing toxin. This could be either the same toxin unlabeled at 10^{-7} M, to assess the nonspecific binding, or PnTx2−6 at $10^{-10}-10^{-6}$ M, to evaluate if it can compete with the radiolabeled toxin for the binding site. To remove the free ^{125}I-labeled toxin, the tissue was vacuum-filtered (synaptosomes) (*12*) or centrifuged at 11000g for 5 min (P2) (*14*). The radioactivity bound to the tissue was measured in a γ radiation counter (1275 mini Gamma Counter, LKB, Wallac).

Molecular Modeling of PnTx2−5 and PnTx2−6 Structures. A search for sequence similarity using NCBI PSI-BLAST (*16*) was performed, but no major similarity was found with any protein that had its structure experimentally determined. Fold recognition of both toxins, using mGenThreader (*17*), did not return any significant hit. The cysteine connectivity pattern of PnTx2−5 and PnTx2−6 was deduced by sequence alignment with all short spider toxins that contain at least eight cysteine residues and whose disulfide bridges were experimentally identified (Figure 7A). Accord-
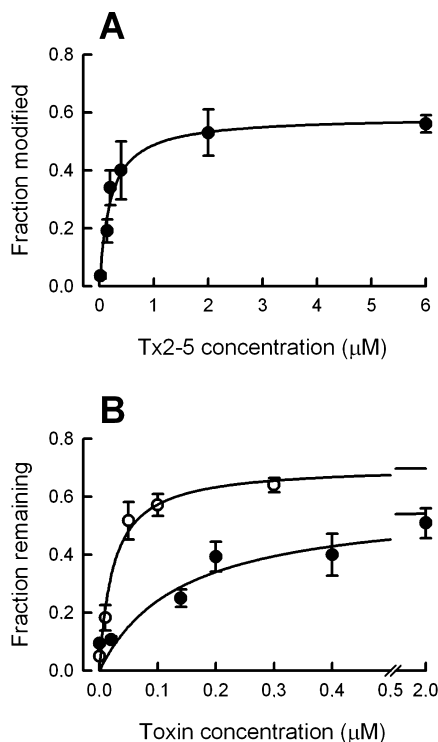
FIGURE 3: Concentration dependence of PnTx2−5 (A) and PnTx2−6 (B). In panel A, the effect was measured by the proportion of the inactivation-modified current calculated by eq 2 (Materials and Methods). The curve is the best fit of the data, with the equation $f(c) = P \times c/(K_{0.5} + c)$, where P is the maximal proportion of modified channels and $K_{0.5}$ is the concentration that modifies half of the channels, having a P of 0.59 and a $K_{0.5}$ of 190 nM. The effect of PnTx2−6 was measured by the current that remained at a time equal to 3-fold the fast time constant of inactivation (○). For the sake of comparison, the same procedure was carried out with the data of PnTx2−5 (●). The curves were obtained by fitting the data with the same equation, with P values of 0.71 and 0.58 and $K_{0.5}$ values of 23 and 140 nM for PnTx2−6 and PnTx2−5, respectively.

ing to SCOP (*18*), CATH (*19*), and DBAli (*20*) databases, they all present the same overall fold, including the so-called inhibitory cystine knot (ICK) structural motif (*21, 22*), with a relatively high degree of conservation of cysteine residue distribution among the group, in spite of the global high degree of sequence variability (*23*). Secondary structure predictions were performed on both target protein sequences using algorithms PHD and PROF (*24*), PSIPRED (*17*), Jpred (*25*), and nnPredict (*26*). Among the group of spider toxins of known structure, template structures were selected according to the following criteria: (i) sequence similarity (using BLAST local alignment algorithm), (ii) secondary structure similarity [by alignment of predicted secondary structures of all toxins, using the SOV algorithm (*27*)], (iii) cysteine pattern similarity [according to spider neurotoxin classification proposed by Kozlov and Grishin (*28*)], and (iv) known target ligand similarity (sodium channel gating modifier toxins). The selected template structures are those from δ-atracotoxin-Hv1 (*29*), δ-palutoxin IT2 (*30*), toxin AcTx-Hi:OB4219 (*31*), and μ-agatoxin-1 (*32*). Their atom coordinates are deposited in the Brookhaven Protein Data Bank (PDB) (*33*) as entries 1VTX, 1V91, 1EIT, and 1KQH, respectively. Three-dimensional structures of PnTx2−5 and PnTx2−6 were calculated by a homology-based molecular modeling method using Modeler 9v3 (*34*). Using the Modeler
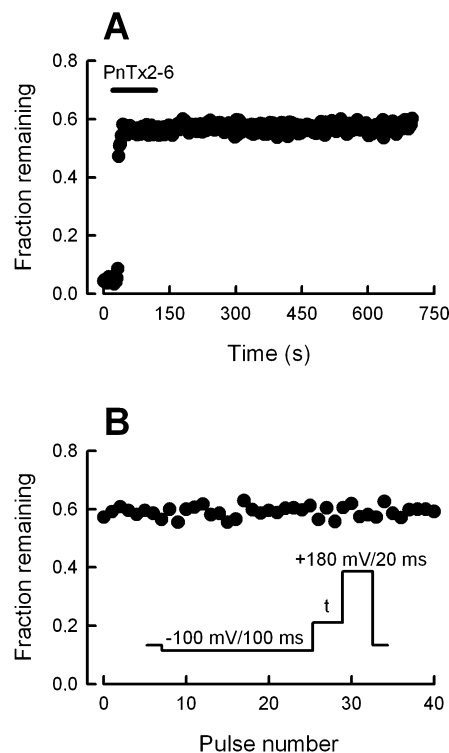

FIGURE 4: Lack of displacement of PnTx2−6 upon washing (A) and upon application of strong (180 mV) depolarizing pulses (B), as shown in the inset, where *t* is the test pulse to 0 mV for 20 ms. The effect was measured with the same procedure described for Figure 3B.
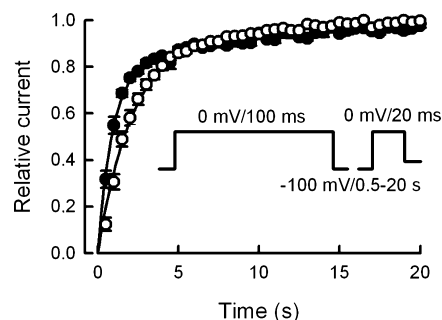

FIGURE 5: Recovery from inactivation in the presence of PnTx2−6. The pulse protocol is shown in the inset. The data were fitted with the sum of two-exponential functions: $f(T) = 1 − [k_1 \exp(−T/\tau_1) + k_2 \exp(−T/\tau_2)]$, where T is the recovery time and k_1 and k_2 are the proportions of the current that recover with time constants τ_1 and τ_2, respectively. The best fits were obtained with the following values: $k_1 = 0.84 \pm 0.04$ and 0.79 ± 0.02, $k_2 = 0.16 \pm 0.04$ and 0.21 ± 0.02, $\tau_1 = 1.99 \pm 0.24$ and 0.91 ± 0.07 s, and $\tau_2 = 4.4 \pm 1.1$ and 10.7 ± 0.8 s in the absence (○) and presence (●) of PnTx2−6, respectively. τ_1 is significantly smaller in the presence of PnTx2−6.

salign command, a structural alignment of the four template structures was generated, and then target sequences of each toxin were aligned together with the resulting structure-based template sequence alignment, using the Modeler *align2d* command. As predicted from target template sequence alignment, the pairs of cysteine residues (Cys3−Cys17, Cys10−Cys23, Cys14−Cys46, Cys16−Cys31, and Cys25−Cys29) from both toxin sequences were virtually constrained to form disulfide bridges. For each toxin, 100 models were calculated and evaluated using Modeler Objective Function (*34*), WHAT IF Check Report results (*35*), Procheck Ramachandran plot analysis (*36*), Verify3D score (*37*), and ProSA z-score (*38*).
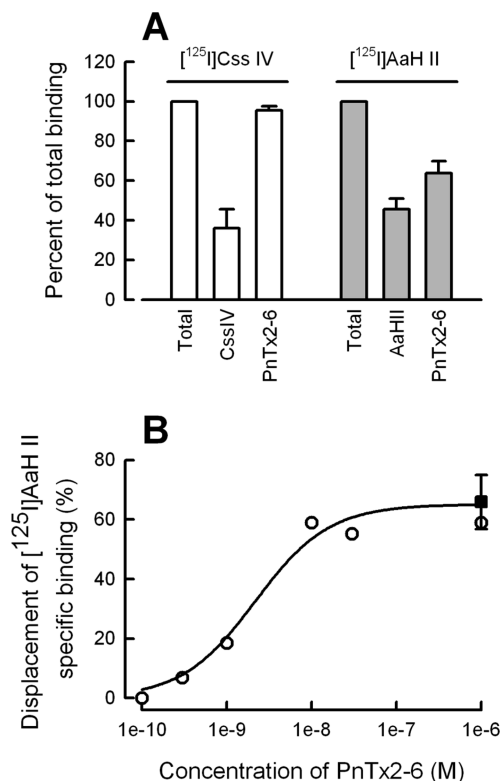
A

B

FIGURE 6: Competition binding assays of PnTx2−6. Panel A shows that PnTx2−6 does not compete with scorpion β-toxin [^{125}I]CssIV and partially competes with scorpion α-toxin [^{125}I]AaHII. In panel B, one experiment carried out in triplicate shows the concentration dependence of the competition for the specific binding. The maximal displacement of specific binding of [^{125}I]AaHII is 58%. The filled square represents the data obtained in the seven independent experiments shown in panel A, replotted as a percentage of displacement of specific binding.

The model which best satisfied the multiple evaluation criteria was selected for each toxin. Electrostatic potentials were calculated using GRASP2 (*39*), and structure representations were drawn using PyMol (*40*).

Statistics. Tests of significance were performed using an unpaired Student's *t* test. The level of significance is $p < 0.05$. Data are shown as averages ± SEM.
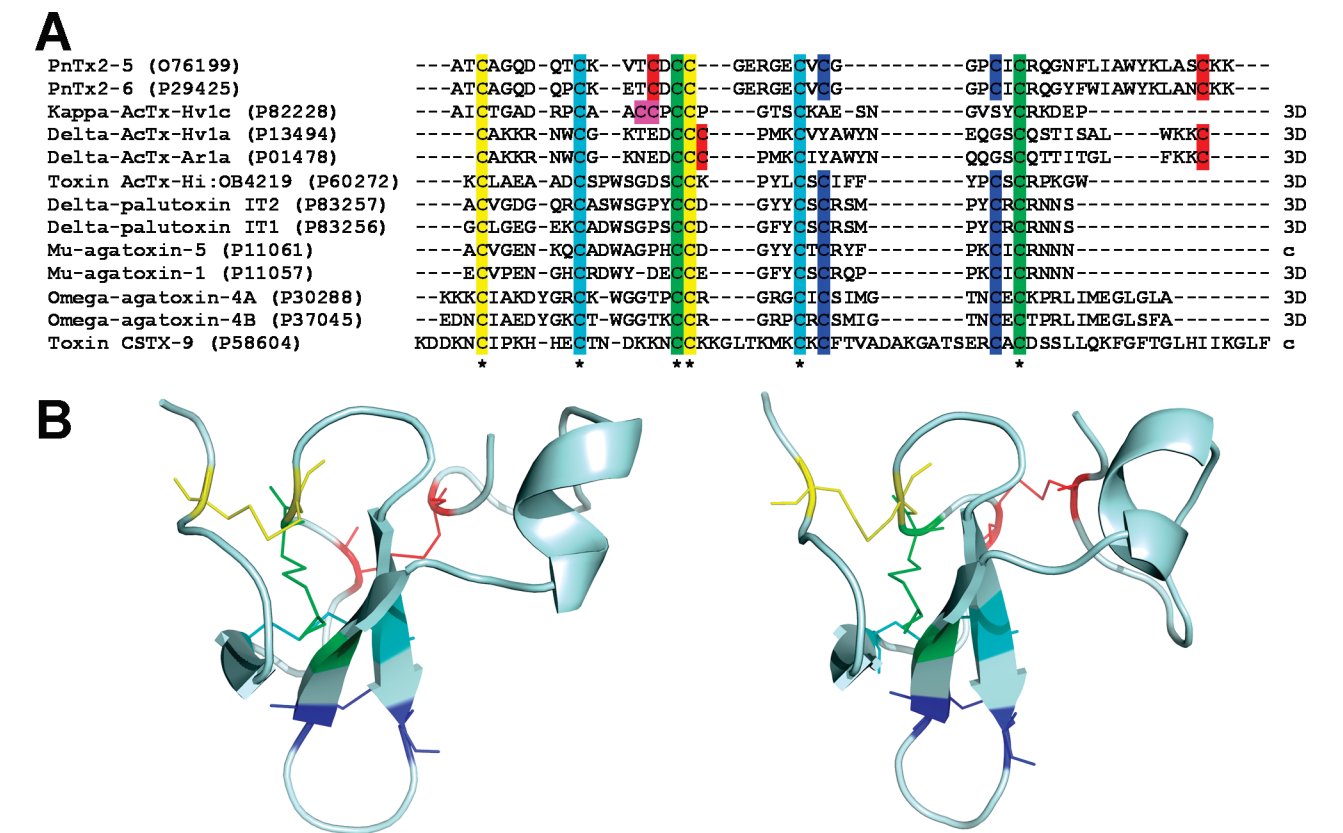
RESULTS

Primary Structures of PnTx2−5 and PnTx2−6. Preliminary assays were needed to decide the correct primary structure of PnTx2−5, whose sequence was first determined by chemical sequencing (*9*). Via examination of a cDNA library constructed from stimulated venom glands, Kalapothakis and collaborators (*41*) were unable to find a sequence that fully matched the reported toxin. A similar sequence was found, in which residue 40 was a tryptophan (instead of an alanine) and cysteine 48 was not present. This sequence was named PnTx2−5a (*41*), because it was uncertain whether it was an isoform of PnTx2−5 or its true sequence. Mass spectroscopy of both toxins used in this work confirmed the expected mass calculated from the PnTx2−6 sequence (5289.31 ± 0.03 Da, calcd 5288.25 Da) and from PnTx2−5a (5112.31 ± 0.41 Da, calcd 5113.1 Da). Since chemical sequencing is prone to errors due to hangover after many cycles of reaction, especially when tiny amounts of material are available, and considering that the purification of our

sample was carried out according to the protocol originally used to purify PnTx2−5, we conclude that its correct sequence is the one shown in Figure 7A, which is identical to the one obtained from cDNA sequencing, while confirming the sequence of PnTx2−6 reported by chemical and cDNA sequencing (see Figure 7A). Furthermore, our data confirm the assumption that all cysteines are oxidized, forming disulfide bridges. Each of these toxins has 48 amino acids, with a 90% level of sequence identity. Using the confirmed sequences, extinction coefficients of 7570 and 14540 M^{-1} cm^{-1} were obtained for PnTx2−5 and PnTx2−6, respectively.

Comparison of PnTx2−5 and PnTx2−6 with Respect to the Na$^+$ Current of GH3 Cells. GH3 cells endogenously express neuronal types of the sodium channel, Nav1.1, Nav1.2, Nav1.3, and Nav1.6 (*42*), whose currents are sensitive to 300 nM tetrodotoxin (not shown). PnTx2−5 and PnTx2−6 modify the Na$^+$ currents in a similar manner, slowing the inactivation kinetics and generating a persistent current at the end of 20 ms pulses (Figure 1A,B). The decrease in the inactivation rate leads to a hyperexcitability and can account for the symptoms of *Phoneutria* envenomation. Preliminary experiments showed no effect on K$^+$ currents. These effects are similar to those produced by scorpion α-toxins, which bind to site 3 of sodium channels. Interestingly, no reversion of the PnTx2−6 effect was observed for up to 10 min after washing out (Figure 4A), in contrast with PnTx2−5 (Figure 1A). Panels D and E of Figure 1 show the normalized current−voltage (*I*−*V*) relationships in the presence of PnTx2−5 and PnTx2−6, respectively. Na$^+$ currents were activated between −35 and −40 mV, while a maximal value near −5 mV was attained under control conditions. The negative shift of the voltage dependence of activation observed in the presence of the toxins is discussed below. In six paired experiments, we observed that addition of PnTx2−5 produced a small (5.2%), but significant, increase in the current amplitude at 0 mV. In seven paired experiments, the effect of 100 nM PnTx2−6 on the current amplitude was not statistically significant.

Effect of P. nigriventer Toxins on the Voltage Dependence of the Na$^+$ Current. To further investigate the negative shift of the Na$^+$ current activation, we calculated the conductance in each potential, normalized for the maximal conductance and plotted as function of the test potential (Figure 2A,B). The points were fitted with a Boltzmann function, and the best fit is shown as a solid line. The potential that activates half of the maximal conductance (V_g) is significantly shifted to negative values in the presence of both toxins. PnTx2−5 at 400 nM shifted V_g by −11.2 ± 0.9 mV ($n = 4$) and PnTx2−6 at 100 nM by −7.8 ± 0.8 mV ($n = 5$).

In addition, we investigated the effect of both toxins on the voltage dependence of steady-state inactivation (Figure 2C,D). Conditioning prepulses (−120 to −25 mV) with a duration of 100 ms were applied and followed by a test pulse to 0 mV, where the currents were measured. Each peak current is normalized to the peak current after the −120 mV conditioning prepulse, and the data were fitted with a Boltzmann function. The best fit is shown as a solid line. As shown in Figure 2C,D, the toxins shifted the V_h to hyperpolarized potentials by −14.0 ± 2.4 mV ($n = 4$) and −20.3 ± 2.9 mV ($n = 5$), in the presence of PnTx2−5 (400 nM) and PnTx2−6 (100 nM), respectively. The slope factor (K_h) was significantly modified by the toxins, and a consider-

A

```
PnTx2-5 (O76199)           ---ATCAGQD-QTCK--VTCDCC---GERGECVCG----------GPCICRQGNFLIAWYKLASCKK---
PnTx2-6 (P29425)           ---ATCAGQD-QPCK--ETCDCC---GERGECVCG----------GPCICRQGYFWIAWYKLANCKK---
Kappa-AcTx-Hv1c (P82228)   ---AICTGAD-RPCA--ACCPCCP----GTSCKAE-SN-------GVSYCRKDEP-------------- 3D
Delta-AcTx-Hv1a (P13494)   -----CAKKR-NWCG--KTEDCCC----PMKCVYAWYN-------EQGSCQSTISAL----WKKC----- 3D
Delta-AcTx-Ar1a (P01478)   -----CAKKR-NWCG--KNEDCCG----PMKCIYAWYN-------QQGSCQTTITGL----FKKC----- 3D
Toxin AcTx-Hi:OB4219 (P60272) ----KCLAEA-ADCSPWSGDSCCK----PYLCSCIFF--------YPCSCRPKGW-------------- 3D
Delta-palutoxin IT2 (P83257) ----ACVGDG-QRCASWSGPYCCD----GYYCSCRSM--------PYCRCRNNS-------------- 3D
Delta-palutoxin IT1 (P83256) ----GCLGEG-EKCADWSGPSCCD----GFYCSCRSM--------PYCRCRNNS-------------- 3D
Mu-agatoxin-5 (P11061)     ----ACVGEN-KQCADWAGPHCCD----GYYCTCRYF--------PKCICRNNN-------------- c
Mu-agatoxin-1 (P11057)     ----ECVPEN-GHCRDWY-DECCE----GFYCSCRQP--------PKCICRNNN-------------- 3D
Omega-agatoxin-4A (P30288) --KKKCIAKDYGRCK-WGGTPCCR----GRGCICSIMG-------TNCECKPRLIMEGLGLA------- 3D
Omega-agatoxin-4B (P37045) --EDNCIAEDYGKCT-WGGTKCCR----GRPCRCSMIG-------TNCECTPRLIMEGLSFA------- 3D
Toxin CSTX-9 (P58604)      KDDKNCIPKH-HECTN-DKKNCCKKGLTKMKCKCFTVADAKGATSERCACDSSLLQKFGFTGLHIIKGLF c
                                 *       *       **  *             *                 *
```

B

FIGURE 7: PnTx2−5 and PnTx2−6 molecular modeling. (A) Sequence and cysteine connectivity pattern of cysteine-rich spider toxins. PnTx2−5 and PnTx2−6 sequences are aligned with all cysteine-rich peptide toxins containing at least eight cysteine residues whose disulfide bridges were experimentally identified, by three-dimensional structure resolution [κ-atracotoxin-Hv1c (*55*), δ-atracotoxin-Hv1a (versutoxin) (*29*), δ-atracotoxin-Ar1a (robustoxin) (*56*), AcTx-Hi:OB4219 (*32*), δ-palutoxins IT2 and IT1 (*30*), μ-agatoxin-1 (*31*), ω-agatoxin-4A (*57*), and ω-agatoxin-4B (*58*)] or by chemical assignment [μ-agatoxin-5 (*59*) and CSTX-9 (*60*)]. Cysteine residues that form disulfide bridges are highlighted with the same color. (B) Cartoon representation of the three-dimensional theoretical models of PnTx2−5 (left) and PnTx2−6 (right). Disulfide bridges Cys3−Cys17, Cys10−Cys23, Cys14−Cys46, Cys16−Cys31, and Cys25−Cys29 are colored yellow, turquoise, red, green, and dark blue, respectively. The amino and carboxy termini are located on the left and right of the molecule, respectively.

Table 1: Ramachandran Plot Statistics of the Template Structures and Models[a]

| | no. of amino acid residues (% of non-Gly non-Pro nonterminal residues) | | | | | |
	1VTX	1V91	1EIT	1KQH	PnTx2−5	PnTx2−6
most favored regions	24 (64.9)	15 (51.7)	18 (62.1)	24 (80.0)	30 (74.4)	32 (84.2)
additional allowed regions	9 (24.3)	13 (44.8)	10 (34.5)	6 (20.0)	7 (20.5)	4 (10.5)
generously allowed regions	3 (8.1)	0 (0.0)	1 (3.4)	0 (0.0)	2 (5.1)	2 (5.3)
disallowed regions	1 (2.7)	1 (3.4)	0 (0.0)	0 (0.0)	0 (0.0)	0 (0.0)
all regions	37 (100.0)	29 (100.0)	29 (100.0)	30 (100.0)	39 (100.0)	38 (100.0)

[a] The table shows, for each structure, the number and percentage of amino acid residues in each dihedral region of the Ramachandran plot (excluding glycine, proline, and the end terminal residues). Data were obtained using Procheck (*36*).

able percentage of channels (15−18%) did not inactivate even with potentials of −25 mV.

Although the effect of PnTx2−5 on the inactivation rate, K_h, and noninactivated fraction were reversible, its effect on V_g was not, while V_h reverted partially upon PnTx2−5 washout (Figure 2A,C).

Sodium Channel Inactivation Kinetics. To characterize the effect of the toxins on the inactivation process, the inactivation rates of the Na$^+$ currents were analyzed. During control inactivation, Na$^+$ currents decay as a single exponential with a fast time constant (390 ± 23 μs). As shown in Figure 1, both toxins inhibit fast inactivation. We fitted the decay of individual currents at 0 mV with a single-exponential function (eq 1) or the sum of two exponentials (eq 2), in the presence of toxins PnTx2−5 and PnTx2−6. The Na$^+$ currents in the presence of either toxin are best fitted with

two exponentials. PnTx2−5 modifies the Na$^+$ currents by adding a slower exponential component (τ_s) to the fast component (τ_f) whose rate remained similar to the control. In contrast, PnTx2−6 slows the fast component (τ_f) in addition to generating a slow component (τ_s) (Figure 1). The same pattern is observed in all potentials where the current decay is dominated by inactivation. We used in our analysis records at 0 mV, because at that potential the sodium conductance has reached its maximum and remains maximal regardless of the voltage shift. In five experiments, the fast time constant of inactivation changed from 0.390 ± 0.023 ms in the absence of PnTx2−6 to 1.21 ± 0.15 ms after addition of PnTx2−6.

Concentration−Response Relationship. Since PnTx2−5 adds a slower time constant (τ_s) to the exponential decay, while preserving a fraction of the current with a fast time
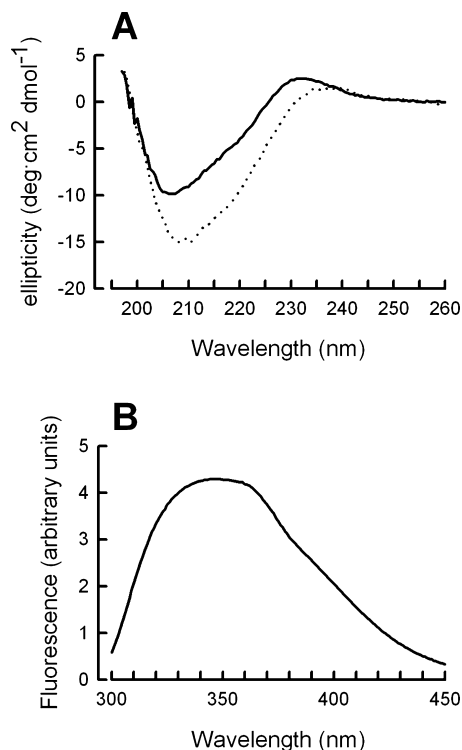
A

B

FIGURE 8: Experimental tests of the proposed model of PnTx2−6. (A) Circular dichroism spectrum of PnTx2−6 (—) compared with the spectrum of ω-atracotoxin Hv1a (*48*) (···). (B) Fluorescence spectrum of PnTx2−6 in water with a maximal fluorescence at 346 nm, consistent with the tryptophan residues being exposed to the hydrophilic medium.

constant (τ_f) whose value is unchanged, it is conceivable that the slow component reflects the toxin-modified channels and the fast component the unbound channels. This interpretation is supported by the experiments shown in Figure 3A. The inactivation kinetics at 0 mV at different concentrations of PnTx2−5 was analyzed, and the relative contribution of the slow component was calculated. The data were initially fitted with a Hill equation [$f(c) = P \times c^n/(K_{0.5}{}^n + c^n)$]. Since the value of n was found to be close to 1, a single-site saturation kinetics was considered and the value of n was fixed as 1. The best fit to the equation is shown as a solid line in Figure 3. The maximal percentage of modified current was 59%, and the concentration of PnTx2−5 that modifies half of the maximal proportion ($K_{0.5}$) was 190 nM. The same reasoning could not be applied to the PnTx2−6 effect, because it modifies the fast time constant (τ_f) besides generating the slow component. To construct a dose−response curve for PnTx2−6, we reanalyzed all curves and measured the fraction of the maximal current that remained after it decayed for a period equal to three time constants of the control. The choice of this time is critical, because it will have a significant effect on the apparent concentration dependence. Our choice was based on the following reasoning. (i) After a time equivalent to three time constants, the contribution of the unmodified channels will be less than 5%. (ii) At that time, the current generated by modified channels will still be high. For the sake of comparison, the effect of PnTx2−5 was also measured with this method and plotted with the results obtained with PnTx2−6 (Figure 3B). The results obtained with PnTx2−5 are similar to those depicted in Figure 3A, supporting the adequacy of the procedure. The graph in Figure 3B was plotted with the best fit obtained with the

same equation, having $K_{0.5}$ equal to 140 and 23 nM, and maximal effects of 58 and 71%, for PnTx2−5 and PnTx2−6, respectively. This means that, in addition to showing reversibility, PnTx2−5 has a $K_{0.5}$ 6 times larger than that of PnTx2−6. The fact that the maximal effect of PnTx2−6 is greater than that of PnTx2−5 may also be meaningful.

Dissociation of the Toxin from the Sodium Channel. We have already shown that PnTx2−5 can be washed off the sodium channel (Figure 1A). In contrast, the effect of PnTx2−6 could not be removed upon washing (Figure 4A). One important characteristic of scorpion α-toxins is that their dissociation from the sodium channel is dependent on the membrane potential and they can be displaced by strong depolarizing pulses (*43−46*). Since the effects of the *Phoneutria* toxins were similar to those of scorpion α-toxins, we used a strong depolarizing pulse after each test pulse to 0 mV to try to dissociate PnTx2−6 from its active site (see the inset of Figure 4B). This protocol was repeated 24 or 40 times (with a 2 s interval) in the absence of free toxin in the external solution. Figure 4B shows that the inhibition of inactivation produced by PnTx2−6 (1 μM) remained even if 40 strong depolarizing pulses (180 mV for 20 ms) were applied alternated with the test pulses, in a medium devoid of the toxin. The rate of dissociation of PnTx2−5 was not significantly altered by the same protocol (not shown).

Although PnTx2−5 and PnTx2−6 differ by only five amino acid residues, they have significant differences in their affinities and binding properties of the sodium channel. We decided to further investigate PnTx2−6, the more potent of these toxins.

Recovery from Inactivation. To characterize the effect of PnTx2−6 on the recovery of sodium channel inactivation, we applied two depolarizing pulses to 0 mV (with a 20 ms duration) separated by a variable interval (from 0.5 to 20 s, with 0.5 s increments), when the membrane was hyperpo-larized to −100 mV (see the pulse protocol in the legend of Figure 5). Figure 5 shows the peak value of the Na$^+$ current during the second pulse normalized by the value of the peak of the current generated by the first pulse and plotted as function of the hyperpolarization time. The curves were fitted with a double-exponential equation, and the best fit is shown as a solid line. In the presence of 500 nM PnTx2−6 (Figure 5), the channels recovered faster from inactivation. Statistical analysis shows that the proportion of each exponential component, k_1 and k_2, was not different from the control, but the time constants of recovery, τ_1 and τ_2, were different.

PnTx2−6 Competition Assay. The effects of PnTx2−6 resemble those of scorpion α-toxins and, less clearly, those of scorpion β-toxins. To determine if PnTx2−6 acts by binding to sites 3 and 4 of the sodium channel, we investigated if it can compete for the binding site of ^{125}I-radiolabeled AaHII and CssIV, typical scorpion α- and β-toxins, respectively. The results depicted in Figure 6A show that PnTx2−6 at a concentration up to 1 μM did not compete with radiolabeled β-toxin CssIV (100 pM) in cortical brain synaptosomes. In a control, excess unlabeled CssIV (100 nM) displaced 64% ($n = 2$) of the radiolabeled toxin, and this percentage is considered the specific binding.

In contrast, PnTx2−6 displaced up to 36% of 100 pM radiolabeled AaHII (Figure 6B) on the fresh P2 fraction of rat brain, whereas the excess of unlabeled AsHII displaced 54%. This means that PnTx2−6 competes partially (67 ±
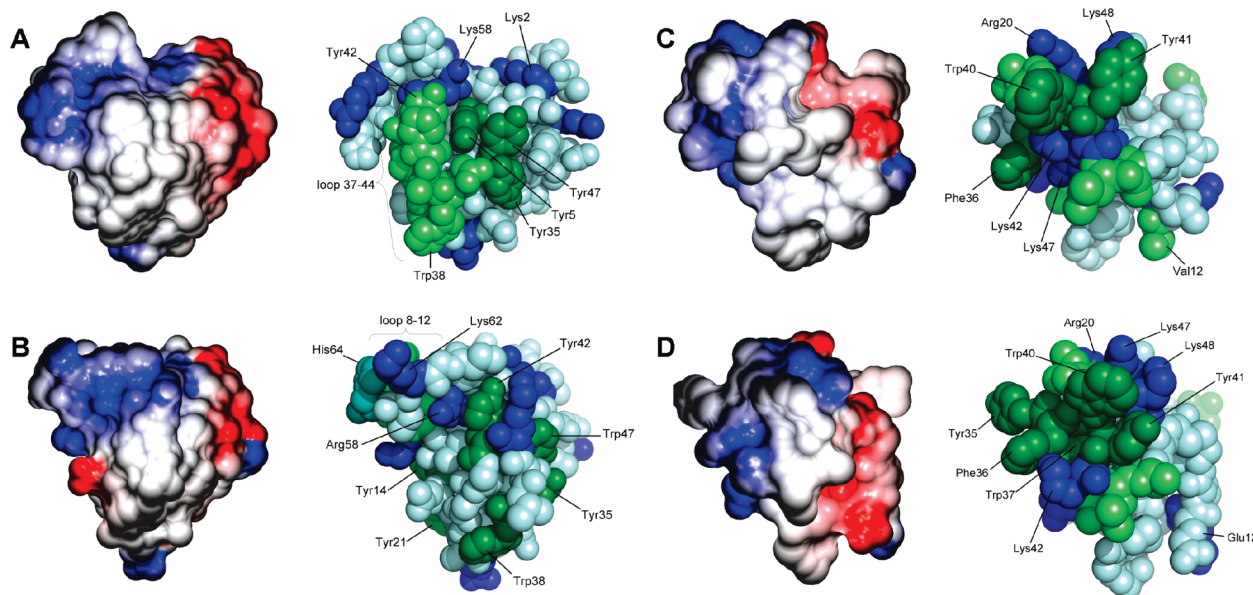
FIGURE 9: Bioactive surface comparison of site 3 mammalian sodium channel modifier neurotoxins AaHII (A), BmKM1 (B), PnTx2−5 (C), and PnTx2−6 (D). Electrostatic potential is mapped to the molecular surface of each molecule structure (left side). The potential is shown at −5.0 to +5.0 kT/e, with k standing for the Boltzmann constant, T the temperature, and e the electron charge. Red indicates regions of negative electrostatic potential; white indicates neutral regions, and blue indicates positive regions. These maps were drawn using GRASP2 (*39*). The sphere representation generated using PyMOL (*40*) is shown for each molecule (right side). Amino acid residues presumed or known to be involved in the interaction with the channel are colored and labeled. Blue denotes positively charged amino acid residues. Hydrophobic residues are colored light green, and aromatic residues are colored dark green.

9%) with AaHII for its specific binding sites. Because the scorpion α-toxin binding depends on the membrane potential, the P2 preparation was found to be more appropriate than synaptosomes, since it better preserves the resting potential of the membrane. When using different concentrations of PnTx2−6 (100 pM to 1 μM), we found that the concentration that attained half of the maximal displacement was 2 nM. It is important to notice that the competition is partial, and the data suggest no tendency toward a complete competition.

Description of the Structures. Figure 7A shows the sequence alignment of PnTx2−5 and PnTx2−6 with 11 cysteine-rich toxins whose cysteine connectivities were experimentally determined. The alignment shows that we can assign to the *Phoneutria* toxins a conserved ICK motif (*21*). A fourth Cys bridge (dark blue) was deduced by similarity, which leads to the fifth pairing (red). Alternative pairings have no resemblance with any known Cys connectivity. Figure 7B shows a cartoon representation of PnTx2−5 and PnTx2−6 molecular models, produced as described in Materials and Methods, with a highlight on the disulfide bridges. The models predict that the three-dimensional structures of PnTx2−5 and PnTx2−6 each contain a short triple-stranded antiparallel β-sheet formed by the Gln8−Cys10, Gly21−Cys25, and Cys29−Gln33 strands and a short α-helix formed by residues 35 (Asn in Tx2−5 and Tyr in Tx2−6) to 39 (Ala in both toxins).

Model Evaluation. The theoretical structures of PnTx2−5 and PnTx2−6 were evaluated with ProSA. Energy plots of PnTx2−5 and PnTx2−6 were found to be similar to those of known structures (not shown). Verify3D evaluation scores of PnTx2−5 and PnTx2−6 structures are rated "relatively good" and similar to those obtained with the evaluation of the experimental structures of the toxins used as a template (not shown). Although some uncommon structural features can be encountered in all template and model structures, analysis by WHAT IF reports that the models show no error

and have properties of good structures (not shown). The Procheck assessment of geometric quality of the structures is shown in Table 1. The results of Ramachandran analysis show that no amino acid residue was found in a disallowed region, and most of the non-Gly and non-Pro nonterminal residues (>74%) lie in the most favored region (Table 1). We noted that the geometric quality of the model structures is even better than that of most of the template structures, except for PDB entry 1KQH. Secondary structure prediction software produced results compatible with both models. These results suggest that the proposed theoretical models can be considered probable structures of toxins PnTx2−5 and PnTx2−6 in solution. In contrast with the scorpion α-toxins, our model predicts a very low content of α-helix. This prediction was verified experimentally by CD analysis of PnTx2−6, as shown in Figure 8A. The observed spectrum supports the proposed model. In fact, the estimated proportion of α-helix using the ellipticity at 222 nm (*47*) is 7.7% (corresponding to 3.7 amino acid residues), which fits well with the proposed model. For the sake of comparison, we also show the experimental CD spectrum of a toxin with a similar experimentally determined structure (ω-atracotoxin Hv1a, PDB entry 1AXH) (*48*). Furthermore, our model predicts that the tryptophan residues are exposed to the toxin surface. This is confirmed by the florescence experiment shown in Figure 8B. Besides being consistent, these models predict characteristics that can be verified experimentally, as discussed.

DISCUSSION

Effects of PnTx2−5 and PnTx2−6 on Neuronal Sodium Channels. Our data clearly demonstrate that toxins PnTx2−5 and PnTx2−6 markedly delay the fast inactivation kinetics of neuronal-type sodium channels (Figure 1B). Similar results with PnTx2−6 were reported on skeletal muscle Na$^+$ currents

using the loose patch clamp technique (*4*), but showing a lower affinity. This effect can account for the prevailing symptoms of *P. nigriventer* envenomation, and despite several similarities with the action of site 3 toxins, important differences exist that may imply differences in their mechanisms of action. In addition, our data show that PnTx2−6 has an affinity 6 times higher than that of PnTx2−5, and its effects are not reversible up to 10 min after washing.

As shown in Figure 2, there is a shift of the voltage dependence of the Na⁺ current in the presence of the toxins, which may suggest an effect similar to that of scorpion *β*-toxins. However, a similar spontaneous shift was described previously in GH3 cells, which tends to reach a maximum of −20 to −25 mV in 30 min (*49*). We found shifts of −11.2 ± 0.9 and −7.8 ± 0.8 mV for the voltage dependence of activation in the presence of PnTx2−5 and PnTx2−6, respectively. After PnTx2−5 had been washed, a shift of −13.4 ± 1.0 mV (relative to the control) was observed, while its effect on the inactivation rate was reverted. The spontaneous shifts measured in four cells maintained under control conditions were −9.3 ± 1.1 and −12.4 ± 1.2 mV, 10 and 15 min after the initial recording, respectively. This is the approximate time of a complete experiment after the whole cell configuration is obtained. We conclude that the observed shift on the activation can be explained by the spontaneous shift and cannot be attributed to a *β*-like effect.

In contrast, the spontaneous shifts observed on the voltage dependence of steady-state inactivation were −6.3 ± 1.2 and −7.4 ± 1.0 mV, at 10 and 15 min, respectively, which are significantly lower than those observed with each toxin. The meaningful difference, along with its partial reversion when PnTx2−5 was washed, leads to the conclusion that both toxins shifted the voltage dependence of inactivation toward more hyperpolarizing potentials.

Both toxins slowed the inactivation kinetics of the Na⁺ current. PnTx2−5 generates a slower component in addition to the normal fast one. On the other hand, PnTx2−6 had a more complex effect on neuronal sodium channels: besides adding a slower component, it also increased the time constant of the fast component (see below).

It is interesting to notice that the data shown in Figure 3 predict that, even at saturating concentrations, a significant proportion of the Na⁺ current (41%) remains unaffected by PnTx2−5. Although alternative explanations cannot be ruled out, this result suggests that part of the population of the sodium channels present in GH3 cells has its inactivation kinetics preserved, implying that PnTx2−5 may not act equally in all channel types expressed in these cells (Nav1.1, Nav1.2, Nav1.3, and Nav1.6). This result differs from what is observed with scorpion α-toxins (*45*) and may be the basis for some differential effects of these toxins, notably the priaptic effect of PnTx2−5. In this respect, the effect of PnTx2−6 is less clear, because of its effect on the fast component of inactivation that may overshadow the possibility that part of the population of sodium channels is resistant to PnTx2−6. A small increase in the time constant of inactivation of part of the population of sodium channels, not sufficiently high to be distinguishable from the unaffected channels, would produce this effect. The incomplete competition observed in Figure 6 reinforces the interpretation that there are neuronal types of sodium channels that bind AaHII, but not PnTx2−6.

It is important to notice that PnTx2−6 reduced the time for the sodium channel to recover from the inactivation state. This effect is similar to that reported for scorpion α-toxins (*46*) and may reflect its mechanism of action, as discussed below.

Mode of Action. The effects described in this paper resemble in many aspects those reported for scorpion α-toxins, namely, the decrease in the inactivation rate, the appearance of a noninactivating current, and the decrease in the time for recovery from inactivation. Furthermore, the experiments depicted in Figure 6 show that PnTx2−6 can displace 67% of the specific binding of AaHII, a typical scorpion α-toxin, while not competing with CssIV (a typical scorpion β-toxin) for its binding site. It is interesting to notice that the ability to displace AaHII is saturated at that level. This means that PnTx2−6 does not bind exactly to the same site (i.e., the same amino acid arrangement) as the scorpion α-toxins, while there may be an overlap. The simplest explanation is that PnTx2−6 cannot bind to all types of sodium channels present in the GH3 cells, while sharing overlapping sites where it can bind. This possibility requires further investigation using heterologously expressed cloned channels.

One striking difference between these toxins is shown in Figure 4B. It is well-known that the site 3 toxins, including sea anemone toxin ATX II, are removed by strong depolarizing pulses, and this property seems intrinsically related to their mechanism of action (*45, 50*). We report for the first time a toxin with effects similar to those of scorpion α-toxins, and possibly overlapping binding sites, that is not removed by strong depolarizing pulses. The affinity of PnTx2−6 is lower than that of the scorpion toxins and cannot account for this absence of displacement. This observation is currently under investigation.

A kinetic model that explains the effect of site 3 toxins was put forward by Campos and collaborators (*45*). This model explains the removal of site 3 toxins and predicts its voltage dependence. It also predicts the recovery from inactivation to be faster in the presence of these toxins, which was confirmed experimentally (*46*). In this work, we show a significant decrease in the time constant of recovery from inactivation in the presence of PnTx2−6 (Figure 5).

We propose that PnTx2−6 binds to a site that overlaps site 3 of the sodium channel, thus producing similar effects on the kinetic properties of the Na⁺ current.

Structural Comparison with Sodium Channel Scorpion α-Toxins. We compared the primary structures of PnTx2−5 and PnTx2−6 toxins with those of scorpion α-toxins and did not find any significant sequence similarity, even in the regions supposed to be participating in the interaction with the channel. However, the possible overlapping binding site of PnTx2−6 and similar electrophysiological properties of PnTx2−5 and PnTx2−6 with scorpion α-toxins prompted us to verify the hypothesis that, despite the lack of sequence similarity, they may have similar bioactive surfaces. It has been shown that scorpion α-toxins have a conserved hydrophobic (predominantly aromatic) core encompassed by basic residues (*51, 52*). Figure 9 shows the comparison of the predicted PnTx2−5 and PnTx2−6 surfaces with the potent α-toxin AahII and with the well-studied scorpion α-like toxin BmKM1, from *Buthus martensii* Karsch. Similar surfaces can be identified, with a conserved hydrophobic

patch surrounded by positive charges. This observation is consistent with the hypothesis that the active surface of gating modifier toxins is an arrangement of hydrophobic and basic residues (*51, 53*). Moreover, of the residues that are nonidentical between the two toxins, two of them are located in the hydrophobic core and are exposed on the surface. One tyrosine (at position 35) and one tryptophan (at position 37), amino acids important for protein−protein interaction (*54*), are absent from the hydrophobic core of PnTx2−5.

The fluorescence data of PnTx2−6 show that the tryptophan residues are exposed to the solvent, as predicted in the models. Aromatic residues Phe36, Trp40, and Tyr41 are also exposed in both toxins. They also contain the same charged amino acid residues, at the same locations. In particular, positively charged residues Arg20, Arg32, Lys42, Lys47, and Lys48 surround the hydrophobic patch in the two structures (Figure 9C,D). This arrangement provides the expected basic requirement for the interaction with site 3 of the sodium channel and conforms to the "recognition patch" found in protein−protein interacting surfaces (*54*). We propose that this charge disposition together with the surrounding aromatic patch (residues Phe36, Trp40, and Tyr41) composes the bioactive surface of PnTx2−5 and PnTx2−6. The additional presence of Tyr35 and Trp37 in PnTx2−6 can account for its higher affinity for the channel.

ACKNOWLEDGMENT

SUPPORTING INFORMATION AVAILABLE

PnTx-5 and PnTx2−6 theoretical model three-dimensional coordinates. This material is available free of charge via the Internet at http://pubs.acs.org.

REFERENCES

1. Billen, B., Bosmans, F., and Tytgat, J. (2008) Animal peptides targeting voltage-activated sodium channels. *Curr. Pharm. Des. 14*, 2492–2502.
2. Campos, F. V., Chanda, B., Beirão, P. S., and Bezanilla, F. (2007) β-Scorpion toxin modifies gating transitions in all four voltage sensors of the sodium channel. *J. Gen. Physiol. 130*, 257–268.
3. Cestèle, S., and Catterall, W. A. (2000) Molecular mechanisms of neurotoxin action on voltage-gated sodium channels. *Biochimie 82*, 883–892.
4. Matavel, A., Cruz, J. S., Penaforte, C. L., Araújo, D. A., Kalapothakis, E., Prado, V. F., Diniz, C. R., Cordeiro, M. N., and Beirão, P. S. (2002) Electrophysiological characterization and molecular identification of the *Phoneutria nigriventer* peptide toxin PnTx2−6. *FEBS Lett. 523*, 219–223.
5. Araújo, D. A., Cordeiro, M. N., Diniz, C. R., and Beirão, P. S. (1993) Effects of a toxic fraction, PhTx2, from the spider *Phoneutria nigriventer* on the sodium current. *Naunyn-Schmiedeberg's Arch. Pharmacol. 347*, 205–208.
6. Monjaraz, E., Navarrete, A., Lopez-Santiago, L. F., Vega, A. V., Arias-Montano, J. A., and Cota, G. (2000) L-type calcium channel activity regulates sodium channel levels in rat pituitary GH3 cells. *J. Physiol. 523* (Part 1), 45–55.
7. Hamill, O. P., Marty, A., Neher, E., Sakmann, B., and Sigworth, F. J. (1981) Improved patch-clamp techniques for high-resolution current recording from cells and cell-free membrane patches. *Pfluegers Arch. 391*, 85–100.
8. Rezende Junior, L., Cordeiro, M. N., Oliveira, E. B., and Diniz, C. R. (1991) Isolation of neurotoxic peptides from the venom of the 'armed' spider *Phoneutria nigriventer. Toxicon 29*, 1225–1233.
9. Cordeiro, M. N., Diniz, C. R., Valentim Ado, C., von Eickstedt, V. R., Gilroy, J., and Richardson, M. (1992) The purification and amino acid sequences of four Tx2 neurotoxins from the venom of the Brazilian 'armed' spider *Phoneutria nigriventer* (Keys). *FEBS Lett. 310*, 153–156.
10. Edelhoch, H. (1967) Spectroscopic determination of tryptophan and tyrosine in proteins. *Biochemistry 6*, 1948–1954.
11. Gill, S. C., and von Hippel, P. H. (1989) Calculation of protein extinction coefficients from amino acid sequence data. *Anal. Biochem. 182*, 319–326.
12. Rochat, H., Tessier, M., Miranda, F., and Lissitzky, S. (1977) Radioiodination of scorpion and snake toxins. *Anal. Biochem. 82*, 532–548.
13. Dunkley, P. R., Heath, J. W., Harrison, S. M., Jarvie, P. E., Glenfield, P. J., and Rostas, J. A. (1988) A rapid Percoll gradient procedure for isolation of synaptosomes directly from an S1 fraction: Homogeneity and morphology of subcellular fractions. *Brain Res. 441*, 59–71.
14. Gray, E. G., and Whittaker, V. P. (1962) The isolation of nerve endings from brain: An electron-microscopic study of cell fragments derived by homogenization and centrifugation. *J. Anat. 96*, 79–88.
15. Lowry, O. H., Rosebrough, N. J., Farr, A. L., and Randall, R. J. (1951) Protein measurement with the Folin phenol reagent. *J. Biol. Chem. 193*, 265–275.
16. Altschul, S. F., Gish, W., Miller, W., Myers, E. W., and Lipman, D. J. (1990) Basic local alignment search tool. *J. Mol. Biol. 215*, 403–410.
17. McGuffin, L. J., Bryson, K., and Jones, D. T. (2000) The PSIPRED protein structure prediction server. *Bioinformatics 16*, 404–405.
18. Murzin, A. G., Brenner, S. E., Hubbard, T., and Chothia, C. (1995) SCOP: A structural classification of proteins database for the investigation of sequences and structures. *J. Mol. Biol. 247*, 536–540.
19. Orengo, C. A., Michie, A. D., Jones, S., Jones, D. T., Swindells, M. B., and Thornton, J. M. (1997) CATH: A hierarchic classification of protein domain structures. *Structure 5*, 1093–1108.
20. Marti-Renom, M. A., Pieper, U., Madhusudhan, M. S., Rossi, A., Eswar, N., Davis, F. P., Al-Shahrour, F., Dopazo, J., and Sali, A. (2007) DBAli tools: Mining the protein structure space. *Nucleic Acids Res. 35*, W393–W397.
21. Craik, D. J., Daly, N. L., and Waine, C. (2001) The cystine knot motif in toxins and implications for drug design. *Toxicon 39*, 43–60.
22. Gelly, J. C., Gracy, J., Kaas, Q., Le-Nguyen, D., Heitz, A., and Chiche, L. (2004) The KNOTTIN website and database: A new information system dedicated to the knottin scaffold. *Nucleic Acids Res. 32*, D156–D159.
23. Conticello, S. G., Pilpel, Y., Glusman, G., and Fainzilber, M. (2000) Position-specific codon conservation in hypervariable gene families. *Trends Genet. 16*, 57–59.
24. Rost, B., Sander, C., and Schneider, R. (1994) PHD: An automatic mail server for protein secondary structure prediction. *Comput. Appl. Biosci. 10*, 53–60.
25. Cuff, J. A., Clamp, M. E., Siddiqui, A. S., Finlay, M., and Barton, G. J. (1998) JPred: A consensus secondary structure prediction server. *Bioinformatics 14*, 892–893.
26. Kneller, D. G., Cohen, F. E., and Langridge, R. (1990) Improvements in protein secondary structure prediction by an enhanced neural network. *J. Mol. Biol. 214*, 171–182.
27. Rost, B., Sander, C., and Schneider, R. (1994) Redefining the goals of protein secondary structure prediction. *J. Mol. Biol. 235*, 13–26.
28. Kozlov, S., and Grishin, E. (2005) Classification of spider neurotoxins using structural motifs by primary structure features. Single residue distribution analysis and pattern analysis techniques. *Toxicon 46*, 672–686.
29. Fletcher, J. I., Chapman, B. E., Mackay, J. P., Howden, M. E., and King, G. F. (1997) The structure of versutoxin (δ-atracotoxin-Hv1) provides insights into the binding of site 3 neurotoxins to the voltage-gated sodium channel. *Structure 5*, 1525–1535.
30. Ferrat, G., Bosmans, F., Tytgat, J., Pimentel, C., Chagot, B., Gilles, N., Nakajima, T., Darbon, H., and Corzo, G. (2005) Solution structure of two insect-specific spider toxins and their pharmacological interaction with the insect voltage-gated Na$^+$ channel. *Proteins 59*, 368–379.

31. Omecinsky, D. O., Holub, K. E., Adams, M. E., and Reily, M. D. (1996) Three-dimensional structure analysis of μ-agatoxins: Further evidence for common motifs among neurotoxins with diverse ion channel specificities. *Biochemistry 35*, 2836–2844.

32. Rosengren, K. J., Wilson, D., Daly, N. L., Alewood, P. F., and Craik, D. J. (2002) Solution structures of the cis- and trans-Pro30 isomers of a novel 38-residue toxin from the venom of *Hadronyche Infensa* sp. that contains a cystine-knot motif within its four disulfide bonds. *Biochemistry 41*, 3294–3301.

33. Berman, H. M., Westbrook, J., Feng, Z., Gilliland, G., Bhat, T. N., Weissig, H., Shindyalov, I. N., and Bourne, P. E. (2000) The Protein Data Bank. *Nucleic Acids Res. 28*, 235–242.

34. Fiser, A., and Sali, A. (2003) Modeller: Generation and refinement of homology-based protein structure models. *Methods Enzymol. 374*, 461–491.

35. Vriend, G. (1990) WHAT IF: A molecular modeling and drug design program. *J. Mol. Graphics 8*, 52–56, 29.

36. Laskowski, R. A., MacArthur, M. W., Moss, D. S., and Thornton, J. M. (1993) PROCHECK: A program to check the stereochemical quality of protein structures. *J. Appl. Crystallogr. 26*, 283–291.

37. Eisenberg, D., Luthy, R., and Bowie, J. U. (1997) VERIFY3D: Assessment of protein models with three-dimensional profiles. *Methods Enzymol. 277*, 396–404.

38. Wiederstein, M., and Sippl, M. J. (2007) ProSA-web: Interactive web service for the recognition of errors in three-dimensional structures of proteins. *Nucleic Acids Res. 35*, W407–W410.

39. Petrey, D., and Honig, B. (2003) GRASP2: Visualization, surface properties, and electrostatics of macromolecular structures and sequences. *Methods Enzymol. 374*, 492–509.

40. DeLano, W. L. (2002) The PyMOL Molecular Graphics System, DeLano Scientific, San Carlos, CA.

41. Kalapothakis, E., Penaforte, C. L., Beirão, P. S., Romano-Silva, M. A., Cruz, J. S., Prado, M. A., Guimarães, P. E., Gomez, M. V., and Prado, V. F. (1998) Cloning of cDNAS encoding neurotoxic peptides from the spider *Phoneutria nigriventer*. *Toxicon 36*, 1843–1850.

42. Vega, A. V., Espinosa, J. L., Lopez-Dominguez, A. M., Lopez-Santiago, L. F., Navarrete, A., and Cota, G. (2003) L-type calcium channel activation up-regulates the mRNAs for two different sodium channel α subunits (Nav1.2 and Nav1.3) in rat pituitary GH3 cells. *Brain Res. Mol. Brain Res. 116*, 115–125.

43. Rogers, J. C., Qu, Y., Tanada, T. N., Scheuer, T., and Catterall, W. A. (1996) Molecular determinants of high affinity binding of α-scorpion toxin and sea anemone toxin in the S3-S4 extracellular loop in domain IV of the Na⁺ channel α subunit. *J. Biol. Chem. 271*, 15950–15962.

44. Chen, H., and Heinemann, S. H. (2001) Interaction of scorpion α-toxins with cardiac sodium channels: Binding properties and enhancement of slow inactivation. *J. Gen. Physiol. 117*, 505–518.

45. Campos, F. V., Coronas, F. I., and Beirão, P. S. (2004) Voltage-dependent displacement of the scorpion toxin Ts3 from sodium channels and its implication on the control of inactivation. *Br. J. Pharmacol. 142*, 1115–1122.

46. Campos, F. V., and Beirão, P. S. (2006) Effects of bound ts3 on voltage dependence of sodium channel transitions to and from inactivation and energetics of its unbinding. *Cell Biochem. Biophys. 44*, 424–430.

47. Chen, Y. H., Yang, J. T., and Martinez, H. M. (1972) Determination of the secondary structures of proteins by circular dichroism and optical rotatory dispersion. *Biochemistry 11*, 4120–4131.

48. Tedford, H. W., Gilles, N., Menez, A., Doering, C. J., Zamponi, G. W., and King, G. F. (2004) Scanning mutagenesis of ω-atracotoxin-Hv1a reveals a spatially restricted epitope that confers selective activity against insect calcium channels. *J. Biol. Chem. 279*, 44133–44140.

49. Fernandez, J. M., Fox, A. P., and Krasne, S. (1984) Membrane patches and whole-cell membranes: A comparison of electrical properties in rat clonal pituitary (GH3) cells. *J. Physiol. 356*, 565–585.

50. Campos, F. V., Chanda, B., Beirão, P. S., and Bezanilla, F. (2008) α-Scorpion toxin impairs a conformational change that leads to fast inactivation of muscle sodium channel. *J. Gen Physiol* (in press).

51. Kharrat, R., Darbon, H., Rochat, H., and Granier, C. (1989) Structure/activity relationships of scorpion α-toxins. Multiple residues contribute to the interaction with receptors. *Eur. J. Biochem. 181*, 381–390.

52. Fontecilla-Camps, J. C., Habersetzer-Rochat, C., and Rochat, H. (1988) Orthorhombic crystals and three-dimensional structure of the potent toxin II from the scorpion *Androctonus australis* Hector. *Proc. Natl. Acad. Sci. U.S.A. 85*, 7443–7447.

53. Takahashi, H., Kim, J. I., Min, H. J., Sato, K., Swartz, K. J., and Shimada, I. (2000) Solution structure of hanatoxin1, a gating modifier of voltage-dependent K⁺ channels: Common surface features of gating modifier toxins. *J. Mol. Biol. 297*, 771–780.

54. Chakrabarti, P., and Janin, J. (2002) Dissecting protein-protein recognition sites. *Proteins 47*, 334–343.

55. Wang, X., Connor, M., Smith, R., Maciejewski, M. W., Howden, M. E., Nicholson, G. M., Christie, M. J., and King, G. F. (2000) Discovery and characterization of a family of insecticidal neurotoxins with a rare vicinal disulfide bridge. *Nat. Struct. Biol. 7*, 505–513.

56. Pallaghy, P. K., Alewood, D., Alewood, P. F., and Norton, R. S. (1997) Solution structure of robustoxin, the lethal neurotoxin from the funnel-web spider *Atrax robustus*. *FEBS Lett. 419*, 191–196.

57. Reily, M. D., Holub, K. E., Gray, W. R., Norris, T. M., and Adams, M. E. (1994) Structure-activity relationships for P-type calcium channel-selective ω-agatoxins. *Nat. Struct. Biol. 1*, 853–856.

58. Reily, M. D., Thanabal, V., and Adams, M. E. (1995) The solution structure of ω-Aga-IVB, a P-type calcium channel antagonist from venom of the funnel web spider, *Agelenopsis aperta*. *J. Biomol. NMR 5*, 122–132.

59. Skinner, W. S., Adams, M. E., Quistad, G. B., Kataoka, H., Cesarin, B. J., Enderlin, F. E., and Schooley, D. A. (1989) Purification and characterization of two classes of neurotoxins from the funnel web spider, *Agelenopsis aperta*. *J. Biol. Chem. 264*, 2150–2155.

60. Schaller, J., Kampfer, U., Schurch, S., Kuhn-Nentwig, L., Haeberli, S., and Nentwig, W. (2001) CSTX-9, a toxic peptide from the spider *Cupiennius salei*: Amino acid sequence, disulphide bridge pattern and comparison with other spider toxins containing the cystine knot structure. *Cell. Mol. Life Sci. 58*, 1538–1545.